JMEPEG (2012) 21:222–230
DOI: 10.1007/s11665-011-9865-8

1059-9495/$19.00

Tensile Properties and Work Hardening Behavior of Laser-Welded Dual-Phase Steel Joints

N. Farabi, D.L. Chen, and Y. Zhou

(Submitted June 27, 2010)

The aim of this investigation was to evaluate the microstructural change after laser welding and its effect on the tensile properties and strain hardening behavior of DP600 and DP980 dual-phase steels. Laser welding led to the formation of martensite and significant hardness rise in the fusion zone because of the fast cooling, but the presence of a soft zone in the heat-affected zone was caused by partial vanishing and tempering of the pre-existing martensite. The extent of softening was much larger in the DP980-welded joints than in the DP600-welded joints. Despite the reduction in ductility, the ultimate tensile strength (UTS) remained almost unchanged, and the yield strength (YS) indeed increased stemming from the appearance of yield point phenomena after welding in the DP600 steel. The DP980-welded joints showed lower YS and UTS than the base metal owing to the appearance of severe soft zone. The YS, UTS, and strain hardening exponent increased slightly with increasing strain rate. While the base metals had multi-stage strain hardening, the welded joints showed only stage III hardening. All the welded joints failed in the soft zone, and the fracture surfaces exhibited characteristic dimple fracture.

Keywords dual-phase steel, fractography, laser welding, microstructure, tensile property, work hardening

1. Introduction

The legislation regarding CO_2 emission reduction via a better fuel economy has urged the car manufacturers to use lighter yet stronger materials which must also meet the safety standards in terms of mechanical properties. In this regard, dual-phase (DP) steel has already gained its popularity as this type of steel has a good combination of higher tensile strength along with significant ductility. The microstructural matrix of DP steel consists of mostly martensitic islands on the ferrite matrix with or without potential bainite and a small amount of retained austenite (Ref 1-5). The ductility of the steel arises from the relatively soft ferrite, and the harder martensite accounts for the strength. Usually DP steel is produced via intercritical annealing followed by rapid cooling (Ref 6, 7). During the intercritical annealing, small pools of austenite are formed in the ferrite matrix, which subsequently transform into martensite upon rapid cooling. The austenite-to-martensite transformation, accompanied by a volume expansion, leads to the occurrence of mobile dislocations into the surrounding ferritic matrix. The mobility of these dislocations is responsible for the high initial work hardening rate and continuous deformation behavior in the DP steels (Ref 6, 8). Therefore, compared with high-strength low-alloy (HSLA) steels, DP steel shows slightly lower yield strength (YS), but the continuous flow behavior in the DP steel results in a larger and more uniform total elongation, and a higher initial work hardening rate along with a considerably higher ultimate tensile strength (UTS) (Ref 9).

The automotive applications of DP steels inevitably involve welding and joining. Owing to flexibility and ease of automation, laser welding has been used increasingly as a joining process of both ferrous (Ref 10, 11) and nonferrous materials (Ref 12, 13) to partially replace some commonly used joining operation in automotive industry, e.g., resistance spot welding (RSW) (Ref 14). However, recent studies showed that the welding led to the formation of a soft zone in the subcritical area of the heat-affected zone (HAZ) and the mechanical properties of the welded joints were affected by this area (Ref 15, 16).

A lot of investigations have been directed toward the mechanical properties and work hardening behavior of DP steels in relation to their microstructure. The tensile properties of these kinds of steels were found to be dependent on the volume fraction (Ref 17, 18), strength (Ref 19), morphology (Ref 20, 21) of martensite and also other factors. Some empirical laws of stress-strain relationship have been used to explain the work hardening behavior of DP steels (Ref 7, 17, 22-24). Among these most popular are Hollomon analysis (Ref 25), and Crussard-Jaoul (C-J) analysis (Ref 26, 27) based on Ludwik (Ref 28) and Swift (Ref 29) equations, popularly known as differential C-J (DC-J) (Ref 30, 31) and modified C-J (MC-J) (Ref 32, 33) techniques, respectively (Ref 20, 24). However, the effect of laser welding on the tensile properties and hardening characteristics of such steels is still limited. Therefore, this study is aimed at evaluating the tensile properties and work hardening behavior with an emphasis on the failure mechanism of the laser-welded DP steel joints under different strain rates.

N. Farabi and **D.L. Chen**, Department of Mechanical and Industrial Engineering, Ryerson University, 350 Victoria Street, Toronto, ON M5B 2K3, Canada; and **Y. Zhou**, Department of Mechanical and Mechatronics Engineering, University of Waterloo, 200 University Avenue West, Waterloo, ON N2L 3G1, Canada. Contact e-mail: dchen@ryerson.ca.

2. Materials and Experimental Procedure

1.2-mm-thick DP600 steel sheet with a galvannealed coating (46 g/m^2 at the top and 47 g/m^2 at the bottom) and 1.2-mm-thick DP980 steel sheet with a galvannealed coating (60 g/m^2 at the top and 67 g/m^2 at the bottom) were selected for this

Table 1 Dual-phase steels selected in this study

Chemical composition	DP600	DP980
C	0.09	0.15
Mn	1.84	1.50
Si	0.36	0.31
Al	0.05	0.05
Mo	0.01	0.006
Cr	0.02	0.02
Cu	0.03	0.02
S	0.005	0.006
P	0.01	0.01

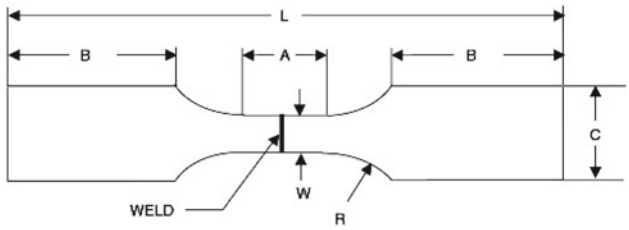

Name	Dimension (mm)
L	140
A	32
W	6
R	6
B	~50
C	9.5
Thickness	1.2

Fig. 1 Geometry and dimensions of the tensile test specimens used in this study

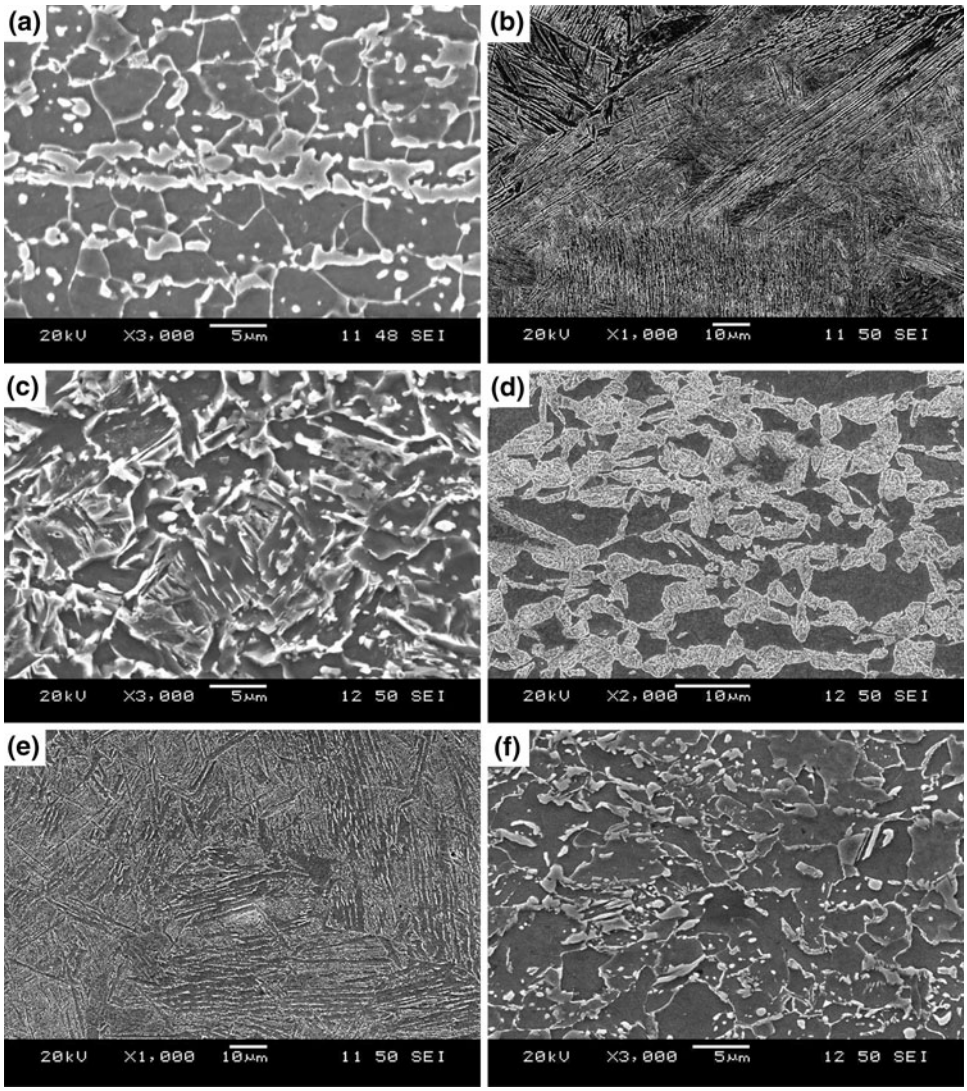

Fig. 2 SEM micrographs showing the microstructural change of a laser welded DP steel joints, (a) DP600 base metal, (b) DP600 fusion zone, (c) DP600 HAZ (soft zone), (d) DP980 base metal, (e) DP980 fusion zone, and (f) DP980 HAZ (soft zone)

Table 2 Welding parameters selected in this study

Laser system	Laser source	Laser power, kW	Welding speed, m/min	Focal length, cm	Beam dimension, mm^2
Nuvonyx ISL-4000	Diode	4	1	9	12×0.9

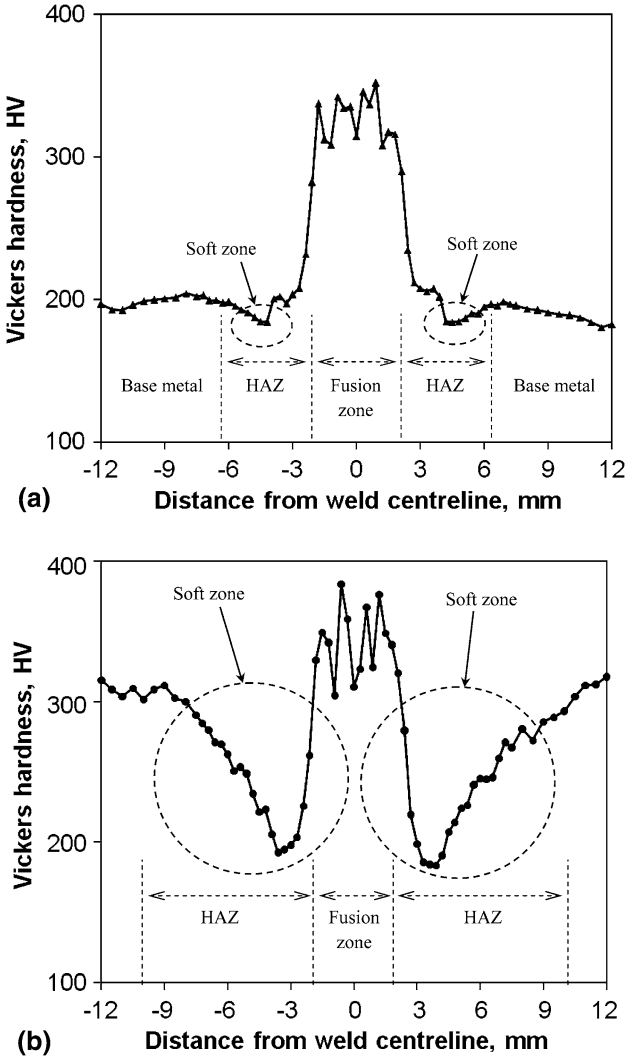

Fig. 3 Typical microhardness profile of the laser-welded (a) DP600 steel joint and (b) DP980 steel joint

study. The chemical compositions of the selected steels are summarized in Table 1. The laser welding was done using a diode laser, and the welding parameters used in this study are shown in Table 2. The diode laser head from Nuvonyx ISL-4000 was mounted on a Panasonic VR6 robotic arm. The beam had a rectangular shape with dimensions of 12×0.9 mm^2 with a focal length of 90 mm. Also, owing to the power density of the diode laser, it was restricted to conduction mode welding. During welding of DP600 steels, ultra-high-purity argon was used as a shielding gas at a flow rate of 16.5 L/min on both surfaces of the blanks, whereas for DP980 sheet welding, the flow rate was 14.2 L/min. Welding was

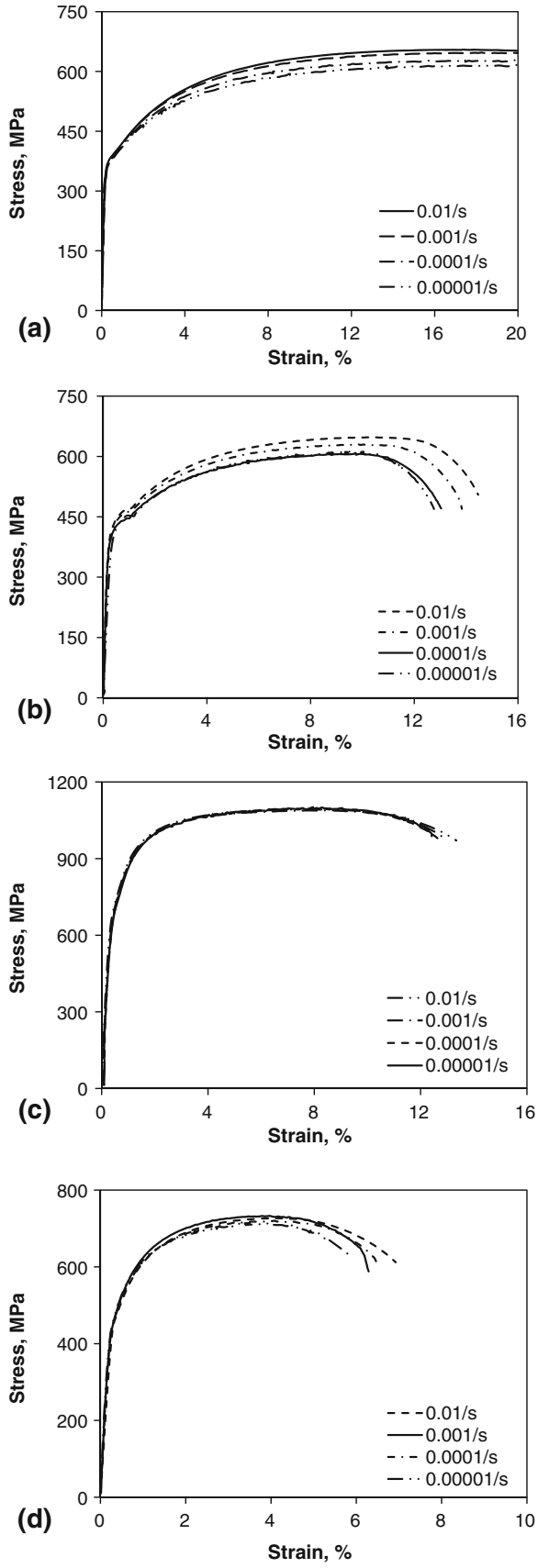

Fig. 4 Engineering stress-strain curves obtained at different strain rates for (a) DP600 base metal, (b) DP600 welded joint, (c) DP980 base metal, and (d) DP980 welded joint

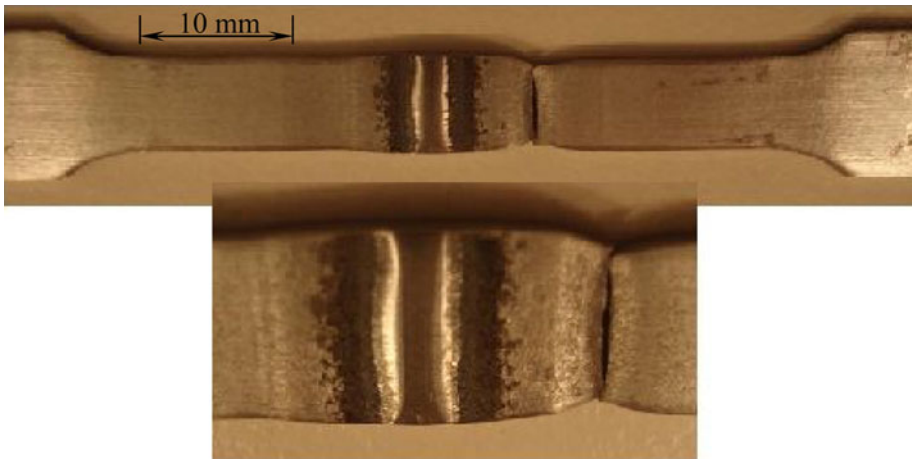

Fig. 5 A typical failed sample after the tensile test for the laser-welded DP980 steel joint

conducted at a welding speed of 1 m/min in full penetration bead on a plate mode.*

Metallographic samples of the welded joints cut perpendicular to the welding direction were prepared and examined using light microscope and scanning electron microscope. Vickers microhardness was determined using a load of 500 g and a dwell time of 15 s. All the microhardness values presented in this study were an average of three series of values taken on the same specimen. The center point of the fusion zone was determined carefully after observing the weld geometry under microscope, and all the indentations were adequately spaced to avoid any potential effect of strain field caused by adjacent indentations.

ASTM-E8M sub-sized specimens were used for the tensile tests. The geometry of the tensile test sample is given in Fig. 1. The welded samples were machined perpendicular to the welding direction. The gauge area of all the test samples was carefully ground along the loading direction with sand papers up to a grit number of 600. Tensile tests were performed at room temperature using a fully computerized universal tensile testing machine. The strain rates selected were 0.01, 0.001, 0.0001, and 0.00001 s^{-1}. An extensometer with a gauge length of 25 mm was used to measure the strain during the test. The 0.2% offset YS, UTS, and ductility (percent elongation) was evaluated, and work hardening rate was analyzed. The tensile fracture surfaces of the base metal and the welded joints were examined via a JSM-6380LV scanning electron microscope equipped with Oxford energy dispersive x-ray spectroscopy (EDS) system.

3. Results and Discussion

3.1 Microstructural Evolution

The SEM micrographs shown in Fig. 2 represent the microstructural evolution that occurred during the welding process. The microstructure of the DP600 base metal can be seen from Fig. 2(a) which contained martensite islands in the ferrite matrix. The SEM examination of fusion zone (FZ) of the laser-welded DP600 indicated that the microstructure in this zone consisted of predominantly martensite in conjunction with some sideplate ferrite and bainite (Fig. 2b). The formation of martensite in the FZ resulted from the rapid cooling of the weld pool during laser welding process. The HAZ of the welded joints contained tempered martensite and bainite in the ferrite matrix which can be seen from Fig. 2(c). Like the DP600 base metal, the micrograph of DP980 base metal can be characterized by martensitic islands in the ferrite matrix (Fig. 2d), but the observed volume fraction of martensite was more compared with DP600. The image analysis indicated that DP600 steel had a martensitic volume fraction of 25% while DP980 steel had a martensitic volume fraction of 52%. Predominantly martensitic phase along with bainite and ferrite sideplates were found to be the microconstituents in the fusion zone of DP980-welded joints, which is shown in Fig. 2(e). The HAZ of these kinds of joints contains tempered martensite along with some possibly bainites in the ferrite matrix (Fig. 2f).

3.2 Microhardness Profile

The microindentation hardness profiles of laser-welded DP600 and DP980 steel joints are shown in Fig. 3(a) and (b), respectively. Significantly higher hardness values, approximately 1.5 times higher than that in the base metal, were observed in the FZ of the welded DP600 joint (Fig. 3a) due to the formation of mostly martensitic structure (Fig. 2b). In the case of welded DP980 steel, the hardness value in the FZ was seen to be slightly higher than that in the base metal. As seen in Fig. 3, a slight decrease (DP600) and a strong decrease (DP980) in the hardness were present in the HAZ, which was called the soft zone. The presence of the soft zone was mainly due to partial disappearance and tempering of pre-existing martensite (Ref 3, 16, 35, 36) which could be seen in Fig. 2(c). The degree of softening in the welded DP980 joints was more severe and the size of the soft zone was also larger than the DP600 steel joints. This is due to the disappearance and tempering of more martensite existing in the DP980 steel.

3.3 Tensile Properties

Figure 4 shows the engineering stress-strain curves obtained from both the base metals and their respective welded joints. Both of the base metals, DP600 and DP980, showed basically smooth and continuous stress-strain curves which could be seen from Fig. 4(a) and (c). However, the DP600-welded joints

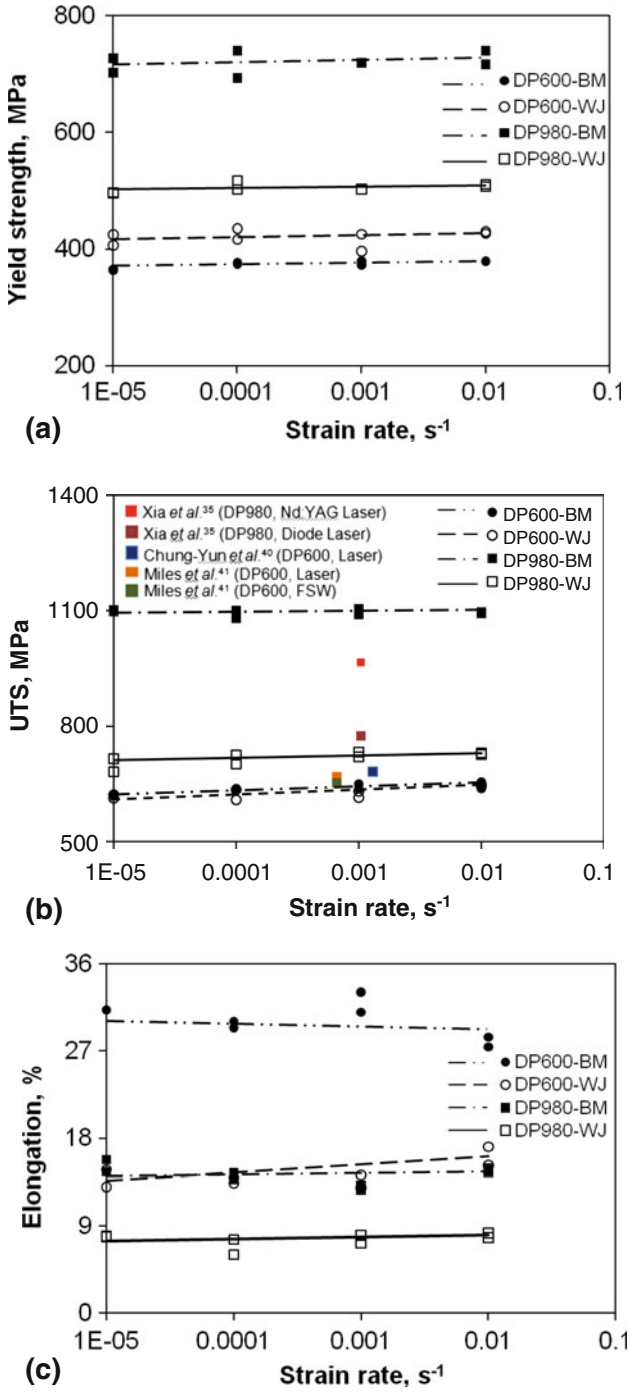

Fig. 6 Effect of laser welding on (a) yield strength (YS), (b) ultimate tensile strength (UTS), and (c) ductility of the DP steels tested at different strain rates

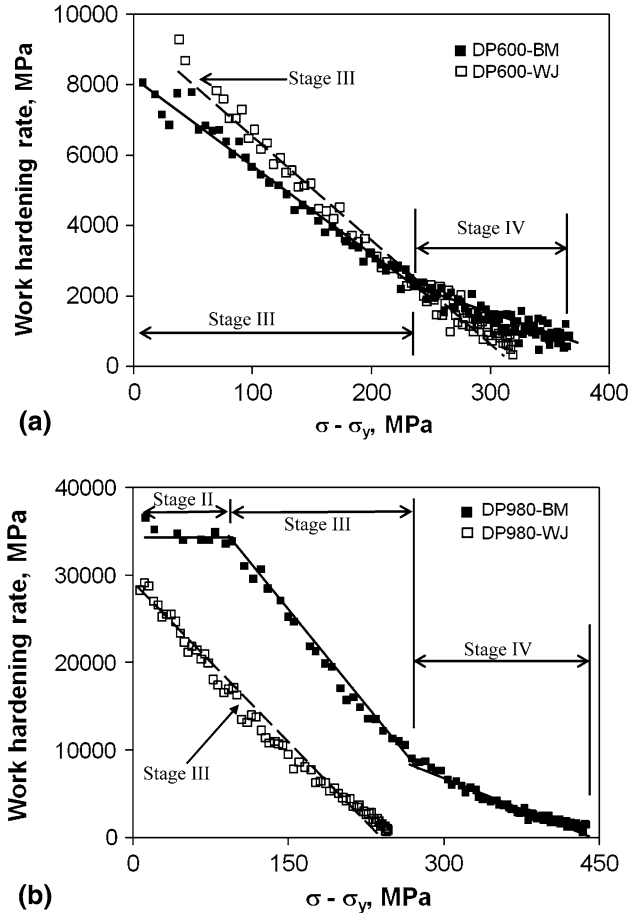

Fig. 7 Work hardening rate vs. net flow stress at a strain rate of 1×10^{-2} s^{-1} for (a) DP600 base metal and welded joint and (b) DP980 base metal and welded joint

exhibited an obvious yield point phenomenon at all the strain rates (Fig. 4b), while the smooth and continuous plastic flow remained in the DP980-welded joints (Fig. 4d). All the welded samples failed in the HAZ with an example shown in Fig. 5 for a welded DP980 tensile sample. Careful observation during the tensile tests showed that the onset of yielding occurred in the softened zone, and then the majority of the plastic deformation was accumulated in that zone (i.e., in the HAZ) until final failure.

The presence of yield point phenomena in the welded samples was likely due to interstitial diffusion which might occur during the laser welding process. The high temperature generated from laser was high enough to drive the carbon or nitrogen atoms in iron to diffuse to the position of high energy just below the extra plane of atoms in a positive edge dislocation. The strong elastic interaction alleviated the impurity atmosphere to become completely saturated and condense into a row of atoms along the core of the dislocation. When such a sample with dislocations pinned by interstitials (i.e., the welded samples in this study) was loaded, a higher stress was required to start the dislocation movement representing the onset of plastic deformation. Once the dislocation line was pulled free from the influence of the solute atoms, slip occurred at a lower stress, exhibiting yield point phenomena (Ref 37-39) as seen in Fig. 4(b).

The effect of laser welding on the YS of the material can be seen from Fig. 6(a). DP600-welded joints were observed to have a higher YS than the base metal due to the presence of yield point phenomena, whereas DP980-welded joints had a lower YS compared with the DP980 base metal. The absence of yield point phenomena and the presence of the more tempered martensite in the HAZ, in conjunction with the partial disappearance of existing martensite, resulted in a reduction in the YS of DP980-welded joints. The UTS of DP600-welded joints was observed to be only marginally lower than that of the base metal, whereas the welding led to a significant reduction in the UTS in the DP980-welded joints (Fig. 6b). The tensile

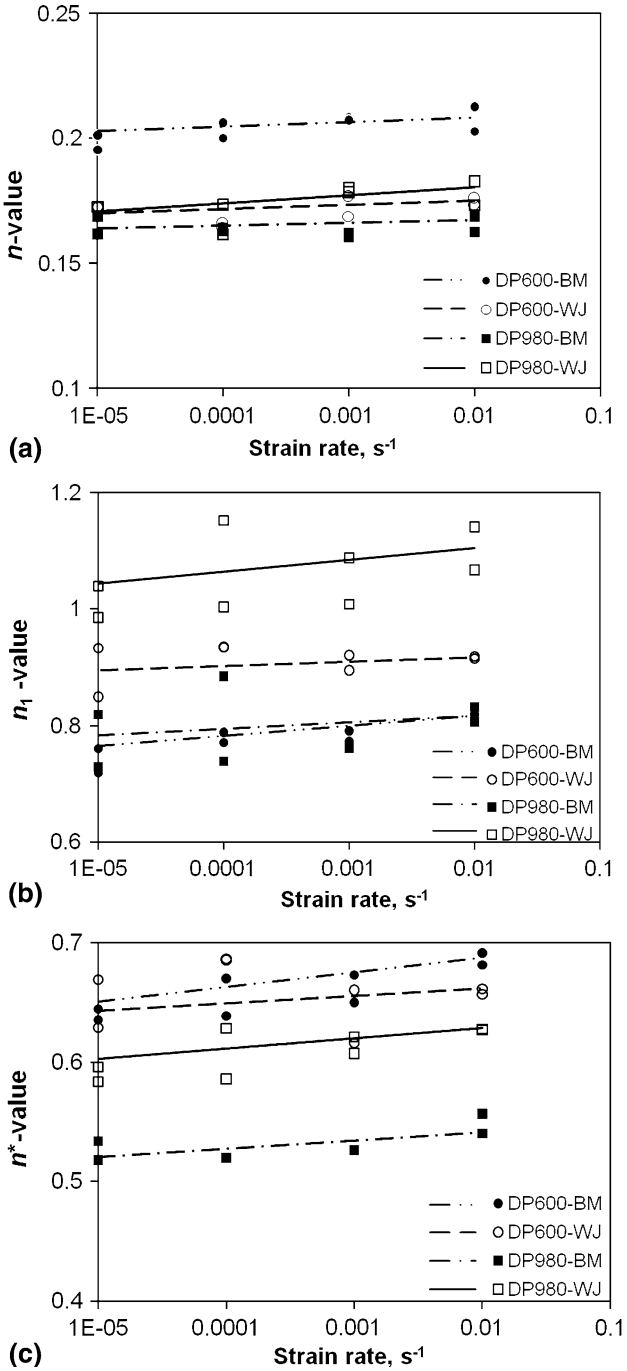

Fig. 8 Work hardening exponents obtained at different strain rates for the DP base metals and welded joints, evaluated according to (a) Hollomon equation (Ref 25), (b) Jaoul-Crussard analysis (Ref 20, 21), and (c) equation proposed by Afrin et al. (Ref 45)

strength of steel is usually related to its hardness. As the degree of softening was very small in the DP600-welded joints (Fig. 3a), the reduction of in the UTS was also hardly visible, but in the case of DP980-welded joints, the degree of softening in the HAZ was significant (about 130 VHN) which eventually resulted in a lower tensile strength in the DP980-welded joints. The strength obtained for both the welded joints in this study was in good agreement with that reported in the literature (Ref 35, 40, 41) (Fig. 6b), in spite of some differences in the welding parameters in different publications.

In all the cases, both the YS and UTS showed only a weak strain rate sensitivity, with the strength increasing by a very small amount with increasing strain rate. At higher strain rates, the dislocation movement was delayed, resulting in increased YS and UTS. Similar kind of increasing trend with increasing strain rate was also reported by Huh et al. (Ref 42) and Samuel (Ref 24) for DP steels. From Fig. 6(c), it can be seen that the DP600 base metal was much more ductile than the DP980 base metal. This was due to the increased martensitic volume fraction in the DP980 steel compared with DP600 steel, as mentioned above. Welding led to a reduction in the elongation of both steels, as seen in Fig. 6(c).

3.4 Work Hardening Behavior

Figure 7 shows a Kocks-Mecking type plot (Ref 43) of strain hardening rate $\theta(=d\sigma/d\varepsilon)$ versus net flow stress $(\sigma - \sigma_y)$ at a strain rate of 1×10^{-2} s^{-1}. Initially DP600 base metal and welded joints showed a similar sort of trend—stage III hardening (Fig. 7a), i.e., θ decreased almost linearly with increasing net flow stress. When the net flow stress exceeded about 240 MPa, the base metal of DP600 steel showed stage IV work hardening behavior despite the small change of the θ value, but it was absent in the DP600-welded joints. Unlike DP600 base metal, DP980 base metal showed a clear stage II work hardening by maintaining almost constant work hardening rate up to a net flow stress of about 120 MPa (Fig. 7b). Then, a linear decrease with increasing net flow stress (i.e., stage III hardening) occurred until the onset of stage IV hardening at a net flow stress of approximately 260 MPa. The occurrences of stage IV hardening in both DP980 and DP600 base steels were in agreement with the observation reported in the literature (Ref 43), where it was reported that stage IV hardening typically appeared in two-phase alloys. Again, like the DP600-welded joints, only stage III hardening occurred in the DP980-welded joints (Fig. 7b). The three stages of work hardening behavior could be understood as follows: In stage II, the constant work hardening rate was due to the deformation of constrained ferrite with possible transformation of retained austenite to martensite (Ref 7, 17, 20). The linear decrease of work hardening rate in stage III arose from simultaneous deformation of ferrite and martensite with attendant cross-slip of dislocations and dynamic recovery of ferrite (Ref 7, 17, 20). In stage IV, the low work hardening rate originated from increased dislocation mobility via profuse cross-slip (Ref 44).

After yielding the stress-strain relationship in the uniform deformation stage could be expressed by Hollomon equation (Ref 25),

$$\sigma = K\varepsilon^n, \qquad \text{(Eq 1)}$$

where σ is the true stress, ε is the true strain, n is the strain hardening exponent, and K is the strength coefficient. The evaluated n values following Eq 1 as a function of strain rate are shown in Fig. 8(a).It is seen that DP600 base metal possessed a higher work hardening exponent than the DP980 base metal. The stronger deformation ability in the DP600 base metal was attributed to the presence of a larger amount of deformable ferrite in the material. With increasing volume fraction of martensite in a DP steel, the value of n usually decreased (Ref 7). After welding, the DP600-welded joints showed a lower work hardening exponent compared with the DP600 base metal. However, the DP980-welded joints had a slightly higher value of n than that of the DP980 base metal.

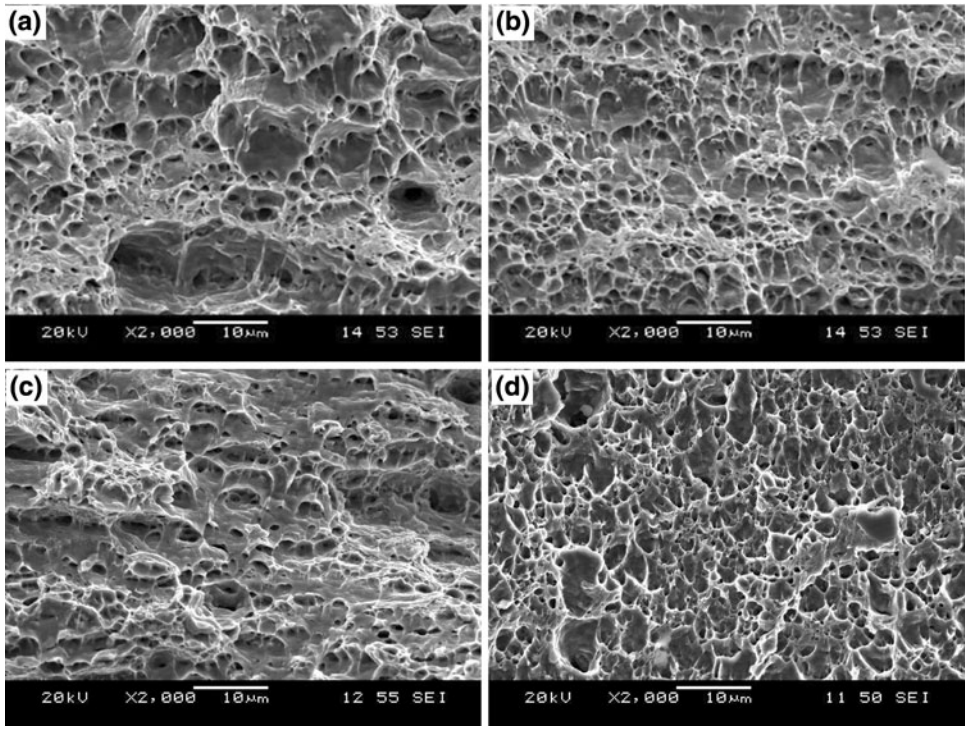

Fig. 9 Typical SEM micrographs of tensile fracture surfaces of the welded joints tested at a strain rate of 1×10^{-2} s^{-1}, (a) center of DP600-welded joint, (b) near-edge area of DP600-welded joint, (c) center of DP980-welded joint, and (d) near-edge area of DP980-welded joint

This might be related to the appreciable softness in the HAZ (Fig. 3b), which would give rise to a higher dislocation storage or hardening capacity. The higher the value of n, the higher the material could be deformed before instability (Ref 37). This could be seen in Fig. 6(c) and 8(a), where a higher n value corresponded to a better ductility in the DP600 steel. In all the cases, the value of n showed only a weak strain rate dependence, i.e., it increased slightly with increasing strain rate.

For better qualification of the strain hardening response, the differential C-J analysis (Ref 26, 27) of the work hardening exponent was used, which was based on the following Ludwik relation (Ref 28),

$$\sigma = \sigma_y + K_1\varepsilon^{n_1}, \qquad \text{(Eq 2)}$$

where σ_y is the yield stress, n_1 is the strain hardening exponent, and K_1 is the strength coefficient which represents the increment in strength due to strain hardening at $\varepsilon = 1$. The evaluation of strain hardening exponent based upon this equation excludes the YS. Figure 8(b) shows the strain hardening exponent n_1 versus the strain rate for both the base metals and the welded joints. Owing to the exclusion of the yield stress in this analysis the work hardening exponents of both the welded joints were seen to become higher than those of the respective base metals. In this study the work hardening exponent was also evaluated according to the following equation proposed recently (Ref 45):

$$\sigma - \sigma_y = K^*(\varepsilon - \varepsilon_y)^{n^*}, \qquad \text{(Eq 3)}$$

where n^*, σ, ε, σ_y, and ε_y are the strain hardening exponent, true stress, true strain, YS, and yield strain of a material, respectively. K^* is the strength coefficient which reflects the increment in strength due to strain hardening corresponding to $(\varepsilon - \varepsilon_y) = 1$. Equation 3 represented the exclusion of both yield stress and yield strain. That is, this relationship reflected the one between net flow stress and plastic strain in the plastic deformation region, in which the elastic deformation stage was no longer included in the evaluation of the strain hardening exponent (Ref 45). The strain hardening exponent n^* evaluated in terms of Eq 3 is shown in Fig. 8(c). It is seen that in all the cases, the values of the work hardening exponents were observed to increase with increasing strain rate to a certain extent. Higher strain rates would lead to a stronger restriction to the dislocation motion which in turn increased the work hardening of a material, since the higher strain rate was observed to generate dislocation morphology with a greater number of tangles in the cell walls and the more refined cell size contributed to stronger work hardening (Ref 46).

3.5 Fractographic Analysis

As mentioned above, the welded joints failed in the HAZ or in the so-called soft zone in all the tensile tests. The fracture surface characteristics were basically similar in both the base metals and their welded joints. Ductile type of failure mode was represented by cup-like dimple rupture which was the main feature of the fracture surface. Typical SEM micrographs of the fracture surface of the welded samples are shown in Fig. 9, in which the center and the edge of DP600-welded samples were shown in Fig. 9(a) and (b) and the similar fracture surface location of DP980-welded samples were illustrated in Fig. 9(c) and (d), respectively. The fracture surface at the center (Fig. 9a, c) contained basically equiaxed dimples indicating typical ductile fracture caused by simple tensile loading. However, careful observations of these two SEM images indicated that the size of the dimples on the fracture surface of the DP600-welded joints (Fig. 9a) was larger than that of the DP980-welded joints (Fig. 9c). This was due to the fact that

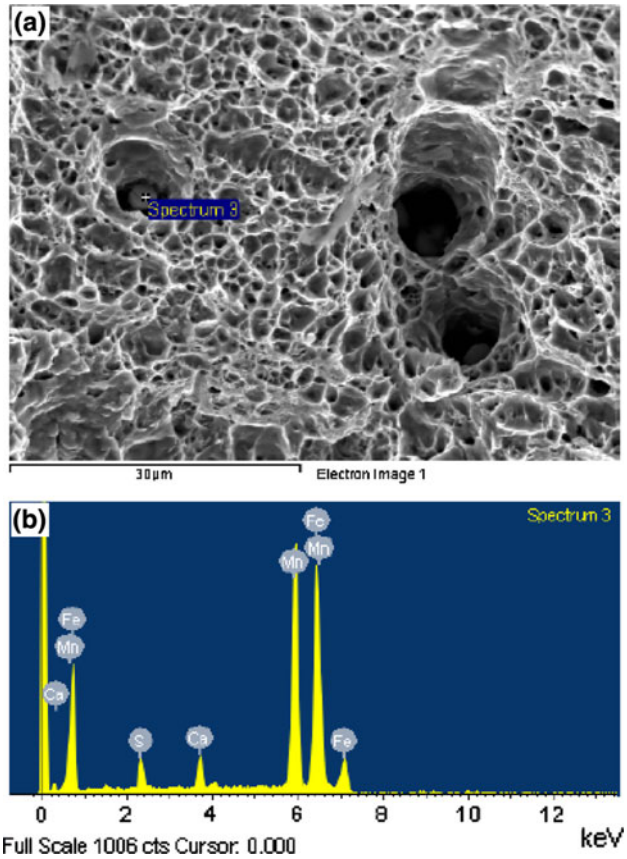

Fig. 10 EDS analysis of particles in the dimples on the fracture surface of a laser-welded DP980 steel joint. (a) A SEM image with larger and deeper dimples and (b) EDS spectrum

the DP600-welded joints contained more deformable ferrite and exhibited a larger elongation than the DP980-welded joints (Fig. 6c). The fracture surface near the edge (Fig. 9b, d) showed a combination of both equiaxed and shear dimples as it had a network of dimpled impressions of equiaxed appearance along with dimples having an elongated parabolic shape indicating the occurrence of shearing motion in conjunction with the simple tensile load. The fracture surface of the welded joints was observed to have some deeper dimples. Energy dispersive x-ray spectroscopic point analysis indicated the presence of manganese-containing particles residing in the deep dimples, as shown in Fig. 10. While the DP980 steel had less manganese content than the DP600 steel (Table 1), the higher carbon content would promote to generate more carbide during welding (Ref 47), which might also be another factor contributing to the lower elongation of the DP980-welded joints (Fig. 6c).

4. Conclusions

1. The laser welding of DP steels resulted in a large amount of martensitic structure formed in the FZ due to the rapid cooling during welding, leading to a considerable increase in the hardness. However, a soft zone in the HAZ was observed due to the partial vanishing and tempering of the pre-existing martensite in the DP steels. The extent of softening and the size of the soft zone were larger in the DP980-welded joints than in the DP600-welded joints.
2. While the presence of the HAZ softening reduced the ductility to a certain extent, the UTS remained nearly unchanged after laser welding in the case of DP600-welded joints. Indeed, the YS of the DP600-welded joints was observed to increase after laser welding due to the presence of yield point phenomena.
3. DP980-welded joints showed lower YS and UTS compared with its base metal due to the significant reduction in the hardness in the HAZ. The ductility also got reduced after welding for both DP steels.
4. The strain rate dependence of the tensile properties was observed to be weak, since the YS and UTS only slightly increased with increasing strain rate from 1×10^{-5} s^{-1} to 1×10^{-2} s^{-1} in both base metals and their welded joints.
5. The base metals of DP steels exhibited multi-stage work hardening, whereas their respective welded joints showed only a single-stage (or stage III) work hardening where the work hardening rate decreased linearly with increasing net flow stress.
6. The work hardening exponents evaluated for both the base metals and the welded joints increased slightly with increasing strain rate, indicating weak strain rate dependence as well.
7. The welded joints tested at different strain rates failed exclusively in the soft zone, and the fracture surface showed ductile fracture characteristics containing mostly dimpled impressions.

Acknowledgments

The authors would like to thank the Natural Sciences and Engineering Research Council of Canada (NSERC), and Initiative for Automotive Innovation (Ontario Research Fund—Research Excellence) for providing financial support. N. F. thanks Ryerson School of Graduate Studies (SGS) for his SGS scholarship. D. L. C. is also grateful for the financial support by the Premier's Research Excellence Award (PREA), Canada Foundation for Innovation (CFI), and Ryerson Research Chair (RRC) program. The authors would also like to thank J. Li (University of Waterloo) for providing the welded joints. and Messrs. A. Machin, Q. Li, J. Amankrah, D. Ostrom, and R. Churaman (Ryerson University) for their assistance in the experiments.

References

1. S.R. Mediratta, V. Ramaswamy, V. Singh, and P. Rama Rao, Microstructure-Mechanical Property Correlations in Dual Phase Steels, *Trans. Ind. Inst. Met.*, 1985, **38**, p 350–372
2. M. Sarwar, E. Ahmad, N. Hussain, B. Ahmad, and T. Manzoor, Crack Path Morphology in Dual-Phase Steel, *J. Mater. Eng. Perform.*, 2006, **15**, p 352–354
3. M. Xia, E. Biro, Z. Tian, and Y.N. Zhou, Effects of Heat Input and Martensite on HAZ Softening in Laser Welding of Dual Phase Steels, *ISIJ Int.*, 2008, **48**, p 809–814
4. D.L. Chen, Z.G. Wang, X.X. Jiang, S.H. Al, and C.H. Shih, Dependence of Near-Threshold Fatigue Crack Growth on Microstructure and Environment in Dual-Phase Steels, *Mater. Sci. Eng. A*, 1989, **108**, p 141–151
5. M. Sarwar and R. Priestner, Fatigue Crack Propagation Behavior in Dual-Phase Steel, *J. Mater. Eng. Perform.*, 1999, **8**, p 245–251

6. R.G. Davies, Influence of Silicon and Phosphorus on the Mechanical Properties of Both Ferrite and Dual-Phase Steels, *Metall. Trans. A*, 1979, **10**, p 113–118
7. T.S. Byun and I.S. Kim, Tensile Properties and Inhomogeneous Deformation of Ferrite-Martensite Dual-Phase Steels, *J. Mater. Sci.*, 1993, **28**, p 2923–2932
8. N.D. Beynon, S. Oliver, T.B. Jones, and G. Fourlaris, Tensile and Work Hardening Properties of Low Carbon Dual Phase Strip Steels at High Strain Rates, *Mater. Sci. Technol.*, 2005, **21**, p 771–778
9. M. Sarwar and R. Priestner, Influence of Ferrite-Martensite Microstructural Morphology on Tensile Properties of Dual-Phase Steel, *J. Mater. Sci.*, 1996, **31**, p 2091–2095
10. H. Kumar, P. Ganesh, R. Kaul, B.T. Rao, P. Tiwari, R. Brajpuriya, S.M. Chaudhari, and A.K. Nath, Laser Welding of 3 mm Thick Laser-Cut AISI, 304 Stainless Steel Sheet, *J. Mater. Eng. Perform.*, 2006, **15**, p 23–31
11. S.K. Samanta, S.K. Mitra, and T.K. Pal, Microstructure and Oxidation Characteristics of Laser and GTAW Weldments in Austenitic Stainless Steels, *J. Mater. Eng. Perform.*, 2008, **17**, p 908–914
12. C. Maletta, A. Falvo, F. Furgiuele, G. Barbieri, and M. Brandizzi, Fracture Behaviour of Nickel-Titanium Laser Welded Joints, *J. Mater. Eng. Perform.*, 2009, **18**, p 569–574
13. M. Marya and G.R. Edwards, Factors Controlling the Magnesium Weld Morphology in Deep Penetration Welding by a CO_2 Laser, *J. Mater. Eng. Perform.*, 2001, **10**, p 435–443
14. H. Tao, W. Tong, L.G. Hector, Jr., and P.D. Zavattieri, Uniaxial Tensile and Simple Shear Behavior of Resistance Spot-Welded Dual-Phase Steel Joints, *J. Mater. Eng. Perform.*, 2008, **17**, p 517–534
15. N. Sreenivasan, M. Xia, S. Lawson, and Y. Zhou, Effect of Laser Welding on Formability of DP980 Steel, *J. Eng. Mater. Technol.*, 2008, **130**, p 041004–041012
16. M. Xia, N. Sreenivasan, S. Lawson, Y. Zhou, and Z. Tian, A Comparative Study of Formability Of Diode Laser Welds in DP980 and HSLA Steels, *J. Eng. Mater. Technol. Trans. ASME*, 2007, **129**, p 446–452
17. A. Bag, K.K. Ray, and E.S. Dwarakadasa, Influence of Martensite Content and Morphology on Tensile and Impact Properties of High-Martensite Dual-Phase Steels, *Metall. Mater. Trans. A*, 1999, **30**, p 1193–1202
18. E. Ahmad, T. Manzoor, K.L. Ali, and J.I. Akhter, Effect of Microvoid Formation on the Tensile Properties of Dual-Phase Steel, *J. Mater. Eng. Perform.*, 2000, **9**, p 306–310
19. H. Chen and G. Cheng, Effect of Martensite Strength on the Tensile Strength of Dual Phase Steels, *J. Mater. Sci.*, 1989, **24**, p 1991–1994
20. D. Das and P.P. Chattopadhyay, Influence of Martensite Morphology on the Work-Hardening Behavior of High Strength Ferrite-Martensite Dual-Phase Steel, *J. Mater. Sci.*, 2009, **44**, p 2957–2965
21. M. Erdogan, The Effect of New Ferrite Content on the Tensile Fracture Behaviour of Dual Phase Steels, *J. Mater. Sci.*, 2002, **37**, p 3623–3630
22. M.R. Akbarpour and A. Ekrami, Effect of Temperature on Flow and Work Hardening Behavior of High Bainite Dual Phase (HBDP) Steels, *Mater. Sci. Eng. A*, 2008, **475**, p 293–298
23. M.S. Nagorka, G. Krauss, and D.K. Matlock, Effect of Microstructure and Strain Rate on the Stage III, Strain Hardening and Ductility of Dual-Phase Steels, *Mater. Sci. Eng.*, 1987, **94**, p 183–193
24. F.H. Samuel, Effect of Strain Rate and Microstructure on the Work Hardening of a Cr-Mo-Si Steel, *Mater. Sci. Eng.*, 1987, **92**, p l5–l8
25. J.H. Hollomon, Tensile Deformation, *Am. Inst. Min. Metall. Eng. Trans. Iron Steel Div*, 1945, **162**, p 268–289
26. B. Jaoul, Etude de Plasticite et Application oux Meatux, *J. Mech. Phys. Solid.*, 1957, **5**, p 95–114
27. C. Crussard, Relationship Between Exact Form of Tensile Curves of Metals and Accompanying Changes in Their Structure, *Rev. Metall.*, 1953, **50**, p 697–710
28. P. Ludwik, *Elements of Technical Mechanics*, Springer, Berlin, 1909
29. H.W. Swift, Plastic Instability Under Plane Stress, *J. Mech. Phys. Solid.*, 1952, **1**, p 1–18
30. S.N. Monteiro and R. Reed-Hill, On the double-n behaviour of iron, *Metall. Mater. Trans. B*, 1971, **2**, p 2947–2948
31. L.F. Ramos, D.K. Matlock, and G. Krauss, On the Deformation Behavior of Dual-Phase Steels, *Metall. Trans. A*, 1979, **10**, p 259–261
32. F.H. Samuel, Tensile Stress-Strain Analysis of Dual-Phase Structures in a Mn-Cr-Si Steel, *Mater. Sci. Eng.*, 1987, **92**, p l1–l4
33. B.K. Jha, R. Avtar, V. Sagar Dwivedi, and V. Ramaswamy, Applicability of Modified Crussard-Jaoul Analysis on the Deformation Behaviour of Dual-Phase Steels, *J. Mater. Sci. Lett.*, 1987, **6**, p 891–893
34. J. Lian, Z. Jiang, and J. Liu, Theoretical Model for the Tensile Work Hardening Behaviour of Dual-Phase Steel, *Mater. Sci. Eng. A*, 1991, **147**, p 55–65
35. M.S. Xia, M.L. Kuntz, Z.L. Tian, and Y. Zhou, Failure Study on Laser Welds of Dual Phase Steel in Formability Testing, *Sci. Technol. Weld. Join.*, 2008, **13**, p 378–387
36. N. Farabi, D.L. Chen, J. Li, Y. Zhou, and S.J. Dong, Microstructure and Mechanical Properties of Laser Welded DP600 Steel Joints, *Mater. Sci. Eng. A*, 2010, **527**, p 1215–1222
37. P. Movahed, S. Kolahgar, S.P.H. Marashi, M. Pouranvari, and N. Parvin, The Effect of Intercritical Heat Treatment Temperature on the Tensile Properties and Work Hardening Behavior of Ferrite-Martensite Dual Phase Steel Sheets, *Mater. Sci. Eng. A*, 2009, **518**, p 1–6
38. G.E. Dieter, *Yield Point Phenomenon, Mechanical Metallurgy, SI, Metric Edition*, McGraw-Hill Book Co., London, 1988, p 197–201
39. W.D. Callister, Jr., *Plastic Deformation, Material Science and Engineering—An Introduction*, 7th ed., Wiley, New York, 2007, p 143–144
40. C.-Y. Kang, T.-K. Han, B.-K. Lee, and J.-K. Kim, Characteristics of Nd:YAG Laser Welded 600 MPa Grade TRIP and DP Steels, *Mater. Sci. Forum*, 2007, **539–543**, p 3967–3972
41. M.P. Miles, J. Pew, T.W. Nelson, and M. Li, Comparison of Formability of Friction Stir Welded and Laser Welded Dual Phase 590 Steel Sheets, *Sci. Technol. Weld. Join.*, 2006, **11**, p 384–388
42. H. Huh, S. Kim, J. Song, and J. Lim, Dynamic Tensile Characteristics of TRIP-Type and DP-Type Steel Sheets for an Auto-Body, *Int. J. Mech. Sci.*, 2008, **50**, p 918–931
43. U.F. Kocks and H. Mecking, Physics and Phenomenology of Strain Hardening: The FCC Case, *Prog. Mater. Sci.*, 2003, **48**, p 171–273
44. J. Cuddy and M. Nabil Bassim, Study of Dislocation Cell Structures from Uniaxial Deformation of AISI, 4340 Steel, *Mater. Sci. Eng. A*, 1989, **113**, p 421–429
45. N. Afrin, D.L. Chen, X. Cao, and M. Jahazi, Strain Hardening Behavior of a Friction Stir Welded Magnesium Alloy, *Scr. Mater.*, 2007, **57**, p 1004–1007
46. W.S. Lee, C. Lin, and B. Chen, Tensile Properties and Microstructural Aspects of 304L Stainless Steel Weldments as a Function of Strain Rate and Temperature, *Proc. Inst. Mech. Eng. C*, 2005, **219**, p 439–451
47. S. Kim, Y. Im, S. Lee, H. Lee, Y.J. Oh, and J.H. Hong, Effects of Alloying Elements on Mechanical and Fracture Properties of Base Metals and Simulated Heat-Affected Zones of SA 508 Steels, *Metall. Mater. Trans. A*, 2001, **32**, p 903–911